Destabilization of the Alzheimer's Amyloid-β Peptide by a Proline-Rich β-Sheet Breaker Peptide: A Molecular Dynamics Simulation Study

Pavan Krishna Kanchi
IIT Guwahati: Indian Institute of Technology Guwahati
Ashok Kumar Dasmahapatra (akdm@iitg.ac.in)
IIT: Indian Institute of Technology Guwahati https://orcid.org/0000-0002-0082-4881

Research Article

Keywords: Amyloid-β fibril, Alzheimer's disease, KLVFF, Molecular dynamics simulations

Posted Date: June 29th, 2021

DOI: https://doi.org/10.21203/rs.3.rs-360999/v1

Version of Record: A version of this preprint was published at Journal of Molecular Modeling on November 18th, 2021. See the published version at https://doi.org/10.1007/s00894-021-04968-x.

Abstract

The amyloid-β peptide exists in the form of fibrils in the plaques found in the brains of patients with Alzheimer's disease. One of the therapeutic strategies is the design of molecules which can destabilize these fibrils. We present a designed peptide KLVFFP$_5$ with two segments: the self-recognition sequence KLVFF and a β-sheet breaker proline pentamer. Molecular dynamics simulations and docking results showed that this peptide could bind to the protofibrils and destabilize them by establishing hydrophobic contacts and hydrogen bonds with a higher affinity than the KLVFF peptide. In the presence of the KLVFFP$_5$ peptide the β-sheet content of the protofibrils was reduced significantly, the hydrogen bonding network and the salt bridges were disrupted to a greater extent than the KLVFF peptide. Our results indicate that the KLVFFP$_5$ peptide is an effective β-sheet disruptor which can be considered in the therapy of Alzheimer's disease.

Introduction

Alzheimer's disease belongs a category of neurodegenerative diseases which is a leading cause of dementia affecting millions of people worldwide, leading to progressive memory loss and cognitive deterioration [1, 2]. This disease is induced by the irregular processing of neuronal proteins [3]. A distinctive feature of this disease is the presence of neuritic plaques in infected brains which are primarily composed of the amyloid fibrils [2, 4]. Neurofibrillary tangles composed of tau proteins are also found in these brains [2, 4]. As a remedy for this disease, molecules with low molecular weights which can cross the blood-brain barrier had been proposed to destabilize the amyloid fibrils and prevent their aggregation [2]. However, since 2003 there have been no new drugs which had been approved, implying that the therapy for this disease is a challenge [5].

In the quest for small molecules which can potentially be therapeutic for Alzhemier's disease, several types of molecules were considered. Chelates and metal coordinations complexes such as iridium (III) and rhodium (III) metal complexes, clioquinol – zinc ion complex, platinum phenanthroline derivatives and Cobalt (III) Schiff bases could inhibit the aggregation of fibrils and diminish their toxicity [6–9]. However in clinical trials the metal chelators PBT1 and PBT2 failed to demonstrate favourable effects [10].

Synthetic compounds such as hexahydropyrroloindoles (HPI), flavone hybrids, triazole-based derivatives, and epigallocatechin-3-gallate (EGCG) could inhibit the aggregation of the fibrils [11–13]. Another class of molecules considered for therapy were antibodies, which displayed insubstantial outcomes due to their large molecular weight as a result of which they were unable to cross the blood-brain barrier [14]. Bapineuzumab and Solanezumab failed in clinical trials [15–17]. However, in patients with mild symptoms, Aducanumab displayed some therapeutic potential [18].

However, most small molecule drugs have some drawbacks. In general, they have a low selectivity for targets, and a poor affinity for the fibrils [19, 20]. Peptide-based drugs have been proposed as an

alternative, due to their ability to have an increased number of interactions with their targets, thereby improving their specificity [20]. Presently, over 100 peptide-based drugs have a market share of about 10% in the ethical pharmaceutical market [20]. They occur frequently as a sequence of 8–10 residues [20]. Apart from their superior specificity, peptide-based drugs are less toxic, possess chemical and biological variety and tend to not gather in tissues [20]. There are some challenges associated with peptide-based drugs. Apart from being metabolically unstable, they have trouble crossing membranes easily [20]. They are mostly delivered by injection as they have poor oral availability [20]. Also, they are associated with inferior solubility and are expensive [20]. If these disadvantages can be prevailed over, peptide-based drugs can show great promise in treating diseases effectively [20].

Peptide sequences obtained from the $A\beta_{1-42}$ peptide can inhibit the aggregation of the $A\beta_{1-42}$ peptides, such as $A\beta_{15-22}$, $A\beta_{16-23}$, and $A\beta_{17-24}$ [21]. The sequence $A\beta_{16-20}$ was recognized as the shortest sequence which initiated the nucleation of the fibrils [22]. This sequence is known as the self-recognition sequence of the amyloid fibrils, and can inhibit the fibrillation process. It was also observed that when the sequence $A\beta_{17-21}$ was modified by the substitutions V17P and A22D, and was injected in the brains of infected rats, it could destabilize the fibrils and arrest their aggregation [23]. Based on these observations, diverse sequences based on the $A\beta_{16-20}$ sequence (KLVFF) were investigated such as adding lysine residues to the KLVFF sequence [24], the $A\beta_{1-28}$ sequence in which the side chains of the residues 17–21 were linked by a lactam linkage and conformationally restrained [25], and the sequences RGKLVFFGR and RGKLVFFGR-NH2 [26]. Other examples of such modifications are the molecules PI-368, PPI-433, PPI-457 [27], polyamine modifications [28, 29], N-methylated sequences [30–34], substitution by D-amino acids [35, 36], linkage to aminoethoxy amide and aspartate [37], the molecules SEN 606, AMY1, AMY2, and K4 [38–40]. The proteolytic stability of the KLVFF peptide was improved by its conjugation with PEG [41].

Amino acids which contain aromatic rings bind to the fibrils with the highest affinity, according to a study by Viet et al [42]. There may be an association between the binding affinity of peptide sequences to amyloid fibrils and their capacity to destabilize amyloid fibrils [42]. Although proline has a five-membered aromatic ring, it has a high binding affinity to the fibrils [42]. Proline has attracted interest in destabilizing amyloid fibrils. Proline-rich polypeptides such as Colostrinin have shown promise in the treatment of Alzheimer's disease by preventing the aggregation of the fibrils in vitro and in clinical studies [43–45]. Another peptide, PRP – 1, which contains four proline residues had shown promise [46]. Proline is a unique residues in the sense that it rarely occurs in beta-sheets [47]. The peptidyl-prolyl bond in proline has a conformation which is not complementary to the geometries of the peptide bond in beta-sheets [48]. The aromatic ring in proline is unable to participate in the hydrogen bonding network of beta-sheets [48]. The internal rotations of the protein backbone depend on the side chains of residues [49]. Proline is a rigid amino acid owing to its pyrrolodine ring which restricts it to accessing fewer conformations [50]. It was shown that when any amino acid in the amyloidogenic sequence LVFFAED was replaced by proline, the sequence became soluble and unable to form fibrils [48].

In the present study, we investigated the ability of a peptide KLVFFPPPPP to destabilize the amyloid protofibrils. In this peptide, denoted as KLVFFP5, the KLVFF sequence was linked to a proline pentamer. This peptide seeks to combine the self-identification and inhibitory property of the KLVFF sequence with the beta-sheet breaker ability of the proline sequence. Five repeat units of proline were selected based on the observation of Murphy et al who in their study of the lysine-modified KLVFF peptide found that three or more repeat units of lysine were more effective [24]. The ability of the KLVFFP5 peptide to destabilize the fibrils and bind to them was compared to the KLVFF peptide. Our results indicate that the KLVFFP5 could disrupt the amyloid protofibrils to a greater extent than the KLVFF peptide and bind more strongly to them.

Methods

The structure of the amyloid-β protofibrils was obtained from the Protein Data Bank (pdb id: 2MXU) [51]. This structure comprises of a triple-parallel S-shaped β-sheet. The three extended β-sheet regions are connected by two loop regions. This model was used in many recent studies [52–58]. The protofibril structure is shown in Fig. 1. The S-shaped structure of the protofibrils used in the present study has greater conformational and mechanical stability [54,59,60] compared to the U-shaped structure of the protofibrils used in previous studies [61,62,63] due to a more robust network of hydrogen bonds [59].

In order to decrease the cost of computation, seven chains of the protofibril structure were considered. Xi et al found that for this model, a protofibril with six chains was the minimum critical size for protofibril stability [64]. They also found that the absence of the first ten residues did not have an impact on the overall protofibril structure. Hence, the choice of the present protofibril structure with seven chains of $A\beta_{11-42}$ is valid for the study.

Neurotoxic oligomers occur in many different sizes. At the begining of the oligomerization of amyloid-β fibrils, the paranuclei consist of pentamers and hexamers which eventually form larger oligomers which later form fibrils [65]. A coarse grained simulation study by Cheon et al showed that pentamers and hexamers are on-pathway intermediates in fibril formation [66]. Another study by Kahler showed that the hexamer is a favourable size for the oligomerization of longer protofibrils [67]. Thus the heptamer model of the protofibrils considered in the present study is a valid target for the design of therapeutic molecules for Alzheimer's disease. Figure 1 shows the model of the protofibrils. For convenience, we refer to the regions shown in the figure as β-1, β-2, and β-3; and loop-1 and loop-2. The β-1 region is spanned by the residues Val 12 – Phe 20, the b-2 region by Asn 27 – Ile 32, and the β-3 region by Val 36 – Ile 41. The chains of the protofibrils are labeled chains A-G; and the ligand as chain H, for convenience.

The systems considered in this study are summarized in Table 1. Three sets of simulations were performed for the following systems: $A\beta_{11-42}$ protofibrils in water, KLVFF- $A\beta_{11-42}$, and $KLVFFP_5$ - $A\beta_{11-42}$. The KLVFF and $KLVFFP_5$ ligands were constructed by PyMol 2.3.1. These ligands were docked to the amyloid protofibrils using the automated protein docking server ClusPro [68–72]. The recommended default procedure was followed in ClusPro. Based on favorable desolvation energies and electrostatics,

the top 2000 models were clustered and ranked by the ClusPro algorithm [71]. The top ranked model was chosen for the present study. The two models chosen for the KLVFF and $KLVFFP_5$ ligands were identically docked to the protofibrils, enabling a basis for the comparison of their effects on the protofibril structure.

Table 1
Summary of systems studied.

System	Composition	Abbreviation
Control System, Replica 1	$A\beta_{11-42}$	C – 1
Control System, Replica 2	$A\beta_{11-42}$	C – 2
Control System, Replica 3	$A\beta_{11-42}$	C – 3
KLVFF – protofibrils, replica 1	KLVFF - $A\beta_{11-42}$	K – 1
KLVFF – protofibrils, replica 2	KLVFF - $A\beta_{11-42}$	K – 2
KLVFF – protofibrils, replica 3	KLVFF - $A\beta_{11-42}$	K – 3
$KLVFFP_5$ – protofibrils, replica 1	$KLVFFP_5$-$A\beta_{11-42}$	KP – 1
$KLVFFP_5$ – protofibrils, replica 2	$KLVFFP_5$-$A\beta_{11-42}$	KP – 2
$KLVFFP_5$ – protofibrils, replica 3	$KLVFFP_5$-$A\beta_{11-42}$	KP – 3

The systems were placed in a cubic box of sizes 7.42543nm (control systems), 7.36071nm (KLVFF systems) and 7.36284nm (KLVFFFP5 systems). The water model used was the TIP3P model. The AMBER99SB-ILDN force field was used for the simulations. In order to neutralize the systems, 7 sodium ions were added to the control systems and 6 to the KLVFF and KLVFFFP5 systems. The steepest descents algorithm was used for energy minimization, followed by equilibriation in two steps with position restraints on heavy atoms. First, an NVT equilibritaion was done for 500ns at 300K, and then an NPT equilibriation was done for 500ns using the Nosé–Hoover temperature bath [73,74] and the Parrinello-Rahman barostat [75,76]. Finally, a molecular dynamics production run was performed for 1000ns (1μs). The GROMACS 5.1.4 package was used for the simulations with periodic boundary conditions applied in all directions [77]. The P-LINCS constraint algorithm was used for bond lengths [78]. The neighbor search cut-off was at approximately 1 nm. The fast smooth particle mesh Ewald summation method was used to calculate the long-range electrostatic interactions and the Fourier grid spacing was 0.16 nm [79].

For analysis, we considered the last 300ns of the simulations. In order to check for artefacts, the minimum distance of a protein system to its periodic image was evaluated. The root mean squared deviation (RMSD), the secondary structure, hydrogen bonds, and the solvent accessible surface area (SASA) were evaluated using the GROMACS tools gmx rms, do_dssp [80, 81], gmx hbond [82], and gmx

sasa [83] respectively. In order to evaluate the sustained contacts, the VMD script contactFreq.tcl was used.

The MM/PBSA method was used to evaluate the binding free energies of the amyloid protofibrils with the ligands. According to the MM/PBSA method, the binding energy is given by the following equation [84, 85] :

$$\Delta G^{bind} = \Delta EMM + \Delta G^{psolv} + \Delta G^{npsolv} - T\Delta S \qquad (1)$$

In Eq. (1), ΔEMM is the molecular mechanics contribution to the binding free energy in vacuum. The polar solvation energy was evaluated by solving the non-linear Poisson-Boltzmann equation and is expressed by the term ΔG^{psolv}. The non-polar contribution to the solvation energy was evaluated by using the solvent-accessible surface area (SASA) model and is given by the term ΔG^{npsolv}. Entropic terms were not considered in the evaluation of the binding energies of the ligands. The tool g_mmpbsa was used for the binding energy calculations employing the single trajectory protocol [86, 87]. Snapshots were extracted every 100ps from the last 30ns of the simulations for analysis. Using 1000 bootstraps in the g_mmpbsa program, individual contributions to the binding energies by the residues were also evaluated. The solute dielectric constant was 4 and the solvent dielectric constant was 80.

Results And Discussion

We describe the binding modes of the KLVFF and $KLVFFP_5$ ligands to the amyloid-β protofibrils in terms of sustained contacts. Sustained contacts are defined as those contacts in which the protofibril residues which were within 4Å of the ligand residues for more than 40% of the last 300ns of simulations. The binding energies of the systems were evaluated along with the contribution of the most important protofibril residues.

Binding Modes

The highest ranked docked structures of the KLVFF and $KLVFFP_5$ systems were chosen. In these structures, the ligands docked to a binding pocket formed by the S-shape of the protofibrils. The binding pocket was evaluated by the web-servers CASTp 3.0, Bitenet and Active Site Prediction [88–90] which use different methods in their calculations. A study by Grasso et al examined the docking of various natural compounds to this particular structure of the protofibrils which was used in the present study [91]. In their study, ligands such as curcumin, gossypin and piceatannol were able bind to this particular binding pocket [91]. Based on these observations, the highest-ranked docked structures produced by the ClusPro algorithm was an appropriate choice for the starting structures of the complexes. The docking of both the ligands was identical, enabling a comparison of their effects on the protofibril structure. The starting structures of the systems and the ligand residues which were within 5Å of the protofibril residues are shown in Fig. 2. KLVFF and $KLVFFP_5$ made contacts with the protofibril residues Val 12, His 13, His 14,

Leu 17, Ile 32, Gly 33, and Leu 34. These residues are in the β-1 region and the loop region Gly 33 – Met 35. These residues correspond to the two binding regions observed by Grasso et al, who found that most ligands tend to bind to the regions E11–F19 and I32–L34 [91]. The KLVFF ligand made contacts with the residues in chains C-G of the protofibrils, while the increased length of the $KLVFFP_5$ ligand enabled it to make contacts with these residues in all the protofibril chains. These residues are highlighted in Fig. 2. The contacts were hydrophobic in nature.

The KLVFF peptide made hydrophobic, hydrogen bonding, and aromatic interactions with the protofibrils. In the last 300ns of the simulations, the KLVFF ligand made eight sustained contacts with the protofibril residues in the K – 1 system. In the K – 1 system, the average number of hydrogen bonds between the KLVFF ligand and the protofibril residues was 3.24. The strong hydrogen bonds between His 14C – Phe 4H lasted for 88% of the time. There were aromatic interactions between Phe 20G – Phe 4H. The prominent contributions to the binding were from the hydrophobic contacts. These residues are shown in Fig. 3 along with their contribution to the binding energy based on the per-residue decomposition of the binding energy term in the last 30ns. The prominent contributions to the binding energy were from Val 12C and His 14C. The contributions to the binding energy are shown in Table 2. The binding energy term was dominated by the van der Waals interactions. The electrostatic interactions were favourable for binding.

Table 2

MMPBSA results expressed in kJ mol^{-1}.

System	van der Waals energy	Electrostatic energy	Polar solvation energy	SASA energy	Binding Energy
K – 1	-186.825 ± 0.958	-943.763 ± 7.976	857.058 ± 6.456	-24.328 ± 0.099	-297.919 ± 3.616
K – 2	-175.002 ± 1.003	-769.843 ± 5.549	762.754 ± 5.191	-23.145 ± 0.101	-205.313 ± 3.285
K – 3	-213.709 ± 1.132	-1501.012 ± 12.067	1347.511 ± 9.156	-29.088 ± 0.095	-396.634 ± 3.707
KP – 1	-213.656 ± 1.160	-1239.946 ± 11.436	1247.314 ± 8.200	-28.845 ± 0.128	-234.845 ± 4.473
KP – 2	-374.728 ± 1.210	-1160.455 ± 8.772	1187.126 ± 5.345	-39.990 ± 0.095	-388.177 ± 4.545
KP – 3	-419.601 ± 1.079	-439.377 ± 4.046	820.437 ± 2.878	-43.269 ± 0.076	-81.957 ± 2.465

In the K – 2 system the KLVFF peptide made 12 sustained contacts with the protofibril residues. The average number of hydrogen bonds between the ligand and the protofibrils in the last 300ns in the K – 2 system was 1.78. The hydrogen bonds between Glu 11C – Val 3H lasted for 82.80% of the time. In the last 150ns, aromatic interactions between Phe 19F – Phe 5H developed. The important contributions to the binding were from the hydrophobic contacts. These are shown in Fig. 3. The Glu 11C residue made

the highest contribution to the binding energy. The contributions to the binding energy are shown in Table 2. The electrostatic interaction and polar solvation energy terms were comparable, implying that the driving force for the binding were the van der Waals interactions. Due to the decrease in favourable electrostatic interactions, this ligand had a lower affinity compared to the K – 1 ligand.

In the K – 3 system the KLVFF ligand made 15 sustained contacts with the fibrils, and made an average of 4.05 hydrogen bonds with the fibrils. Due to a greater number of contacts made with the fibril residues, an increased number of hydrogen bonds, and more favourable electrostatic interactions, the ligand in this replicate had a higher binding affinity for the fibrils than in the K – 1 and K – 2 systems.

In the last 300ns, the $KLVFFP_5$ ligand made 15 sustained contacts with the protofibril residues in the KP – 1 system. The average number of hydrogen bonds between the ligand and the protofibrils was 2.75. The prominent hydrogen bonds were between Glu 22A – Lys 1H (50.10%), Glu 22A – Leu 2H (27.20%), and Asp 23A – Lys 1H (23.60%). As these residues were charged, they contributed significantly to the binding energy, as shown in Fig. 4. The hydrophobic contacts made an important contribution to the binding, the Ile 32D - Pro 9H contact in particular. The contributions to the binding energy are shown in Table 2. The electrostatic interaction and polar solvation energy terms were comparable, implying that the binding was driven by the van der Waals interactions.

In the KP – 2 system, the $KLVFFP_5$ ligand made 27 sustained contacts with the protofibril residues. This was significantly more than the other systems. The average number of hydrogen bonds between the ligand and the protofibrils was 3.73. The important hydrogen bonds were those between Glu 11A – Lys 1H (54.80%), Val 12A – Lys 1H (84.80%), Val 12A – Leu 2H (93.70%), and Glu 11G – Pro 9H (39.20%). Most of the sustained contacts were hydrophobic in nature. The prominent aromatic interaction was between Phe 19F - Phe 5H. The Glu 11A – Lys 1H contact was electrostatic in nature. Important contributions to the binding energy were made by the protofibril residues Glu 11A, Val 12A, His 13A, His 14A, Val 12B, His 14D, Ile 32E, and Glu 11G, as shown in Fig. 4. The contributions to the binding energy are shown in Table 2.This ligand had the highest binding affinity compared to the other systems. The electrostatic interactions were not favourable for binding, and hence the binding was driven by the van der Waals interactions. The high number of hydrophobic contacts made by the ligand contributed significantly to the binding of the $KLVFFP_5$ ligand to the protofibrils. This ligand made more contacts with the protofibril residues than the ligand in the KP – 1 system, and hence had an increased binding affinity. In the case of the KP – 3 system, the ligand residues made 21 sustained contacts with the fibril residues. Due to the relatively low magnitude of the electrostatic interaction energy term and the high magnitude of the polar solvation energy term, the binding affinity was low.

The proline residues in the $KLVFFP_5$ ligands were able to form hydrophobic interactions with the protofibril residues. The proline residues contributed to 5 sustained contacts in the KP – 1 system and 7 sustained contacts in the KP – 2 system. These favourable interactions contributed to the overall binding affinity of the ligand. The high affinity of proline residues to the amyloid protofibrils had been observed in a previous study [42]. In the K – 1 and K – 2 systems the Phe 4H residue made the maximum sustained

contacts with the protofibril residues. In comparison, the residues other than the Phe 4H in the KLVFF sequence in the $KLVFFP_5$ ligands in the KP – 1 and KP – 2 systems bound more tightly to the protofibrils by making more contacts. Thus the proline modification to the KLVFF peptide enhanced its binding to the protofibrils.

Destabilization of the protofibrils

In the presence of the KLVFF and $KLVFFP_5$ ligands the protofibrils became destabilized. The final snapshots of the simulations are shown in Fig. 5. In the absence of the ligands, the protofibrils were stable and maintained their β-sheet structure, hydrogen bonding network and their salt bridges. The extent of destabilization of the protofibrils was the maximum in the presence of the $KLVFFP_5$ ligand in the KP – 1 and KP – 2 systems. The KP – 3 system was an outlier due to the poor binding of the ligand to the fibrils.

The all-atom root mean squared deviation (RMSD) of the Cα atoms of the Aβ protofibrils was evaluated in order to monitor the time evolution of their structural stability. The Aβ protofibril control systems were stable and had average RMSD values of 0.49 ± 0.01nm, 0.48 ± 0.01nm, and 0.58 ± 0.02 nm respectively in the last 300ns. These are shown in Fig. 6.

The destabilization of the protofibrils in the presence of inhibitors was indicated by an increase in the RMSD value of the protofibrils. In the presence of the KLVFF and $KLVFFP_5$ ligands, the RMSD values of the protofibrils had increased. The average RMSD values of the Aβ protofibrils in the KLVFF-Aβ systems had increased to 0.58 ± 0.04 nm, 0.82 ± 0.06 nm, and 0.69 ± 0.04 nm, respectively, indicating the destabilizing effect of the KLVFF peptide. In the KP – 1 and KP – 2 systems, the average RMSD values of the Aβ protofibrils further increased to 0.90 ± 0.04nm and 0.83 ± 0.04nm. The increased values of the RMSD indicate that the $KLVFFP_5$ peptide could destabilize the Aβ protofibrils to a greater extent than the KLVFF peptide in the KP – 1 and KP – 2 systems. The RMSD values as a function of time are shown in Fig. 6.

The average RMSD values of the three extended β-strand regions β − 1, β − 2 and β − 3 were evaluated in order to determine which region was destabilized by the ligands to the highest extent. The ligands in all the systems made more contacts with protofibril residues in the β − 1 region, and subsequently, this region was destabilized to a greater extent. The KLVFF – Aβ systems had higher average RMSD values in the β-1 region than the controls, and these values were even higher for the KP – 1 and KP – 2 systems. The RMSD values of the residues in the β-2 regions of the systems were comparable. The increased RMSD values show that both KLVFF and $KLVFFP_5$ peptides could destabilize the Aβ protofibrils, with the latter destabilizing the protofibrils to a greater extent in the KP – 1 and KP – 2 systems. The $KLVFFP_5$ peptide could destabilize the protofibrils in the β − 1 region (in the KP – 1 and KP – 2 systems), the β − 2 region (in the KP – 2 system), and the β − 3 region (in the KP – 1 system) to a greater extent than the KLVFF peptide. These values are shown in Fig. 7.

The destabilization of the protofibrils was further evaluated by the effect of the ligands on the secondary structure of the Aβ protofibrils. There was a reduction in the β-sheet content of the protofibrils in the presence of both ligands, indicating their ability to destabilize the protofibrils. In the control Aβ systems, the percentage of residues which formed a β-sheet was 45.91%, 52.55% and 41.87% respectively. In the KLVFF - Aβ systems, these values were 42.20%, 42.38%, and 36.66% respectively, indicating a reduction in beta-sheet content compared to the C – 1 and C – 2 systems. In the KP – 1 and KP – 2 systems there was a further reduction of the β-sheet content to 28.02% and 35.27% respectively. The drastic reduction in the β-sheet content of the protofibrils in the presence of the $KLVFFP_5$ peptide indicates the improved destabilization ability of the proline enhancement of the KLVFF peptide. The number of protofibril residues which formed random coils increased in the presence of these peptides. The percentage of residues which formed coils in the control Aβ systems was 34.14%, 28.69%, and 36.42% respectively. These values increased to 39.21% and 37.04%, and 38.58% in the KLVFF-Aβ systems and 39.46% and 39.52% in the KP – 1 and KP – 2 systems. These values are shown in Fig. 8.

The presence of the $KLVFFP_5$ peptide induced the formation of 3_{10} helices and α-helices in the Aβ protofibrils. In the KP – 2 system, the helices were observed in the residues 25–29 of chain A; and the residues in the two regions 20–27 and 34–37 in chain G. In the KP – 3 system, the helices were observed in the residues 21–23 of chain A. A plot of the helix-forming residues as a function of the percent duration of the total simulation time is shown in Fig. 9. 3_{10} helices were more prominent in chains A of the systems KP – 1 and KP – 2; while in chain G of the KP – 1 system, α-helices were more prominent.

A reduction in the number of hydrogen bonds in the presence of the ligands was an indication of the destabilization of the amyloid protofibrils. The $KLVFFP_5$ peptide in the KP – 1 and KP – 2 systems was able to modify the hydrogen bonding network to a greater extent than the KLVFF peptide, as shown in Fig. 10, which shows the average number of hydrogen bonds in the amyloid-β protofibrils in the last 300ns. According to the figure, the average number of hydrogen bonds was the maximum in the systems with the fibrils alone, and the least in the KP – 1 and KP – 2 systems. The hydrogen bonds between neighbouring chains in the systems were further evaluated. The interchain hydrogen bonds which were disrupted by the KLVFF and $KLVFFP_5$ peptides were those between chains D-E, E-F and F-G. Figure 11 shows the average number of inter-chain hydrogen bonds in all the systems considered. The average number of interchain hydrogen bonds between the chains E-F and F-G in the K – 1 and K – 2 systems was less than the controls. In the KP – 1 and KP – 2 systems, the number of hydrogen bonds reduced even further. The average number of interchain hydrogen bonds between chains A-B, B-C, and C-D were comparable in all the systems considered. Since hydrogen bonds play an important role in the stabilization of the amyloid fibrils, a disruption of these indicates the destabilization of the fibrils in the presence of the ligands. These results indicate that the $KLVFFP_5$ peptide could disrupt the hydrogen bonding network of the amyloid protofibrils to a greater extent than the KLVFF peptide.

Salt bridges are important for the stability of the amyloid fibrils [92]. In the solid state NMR studies from which the structure of the amyloid protofibrils used in the present study was obtained, it was observed

that the stabilization of the salt bridge between Lys 28 and Ala 42 was responsible for the S-shaped triple β-sheet motif [51]. This salt bridge is thought to function as a self-recognition molecular switch in the oligomerization of the fibrils [51]. The $KLVFFP_5$ peptide was able to weaken these salt-bridges to a greater extent than the KLVFF peptide in the KP – 1 and KP – 2 systems resulting in the destabilization of the protofibril structure. The average distance between the salt-bridge forming residues and the fraction of the time in which they were within 4Å of each other was measured to characterize the salt-bridges. The salt bridges in the K – 1 system were well preserved. In the K – 2 system, the salt bridges between the chains C – D, D – E, and F – G were disrupted. In the KP – 1 system, the salt bridges which were disrupted were those between chains A-B, and D-E. The salt bridges in the KP – 2 system were disrupted to the greatest extent compared to the other systems. The average distance between the Ala 42- Lys 28 residues was greater than 4Å between all the chains. The 42E – 28F salt bridge was completely lost. The 42B – 28C and 42F – 28G salt bridge-forming residues were in contact with each other for a negligible fraction of time. Disruption of the other salt bridges was also observed. Figures 12 and 13 show the average distance between the salt bridge-forming residues and the fraction of time in which they were within 4Å of each other.

The tight interatomic packing of the protofibrils was made looser in the presence of the KLVFF and $KLVFFP_5$ peptides. The average values of the radius of gyration and the solvent-accessible surface area increased in the presence of the peptides. This indicates that the protofibrils were less compact and more exposed to the solvent in the presence of the $KLVFFP_5$ peptide. These values were the highest in the presence of the $KLVFFP_5$ peptide as shown in Table 3.

Table 3
Radius of gyration and solvent-accessible surface areas (SASA) of the protofibrils.

System	Radius of gyration (nm)	SASA (nm^2)
C – 1	1.66	100.78
C – 2	1.66	103.23
C – 3	1.67	104.32
K – 1	1.70	111.74
K – 2	1.69	109.14
K – 3	1.68	111.71
KP – 1	1.72	115.98
KP – 2	1.73	115.55
KP – 3	1.69	108.68

By disrupting interactions which are critical for the stability of the profibrils, the KLVFF and $KLVFFP_5$ ligands were able to destabilize the protofibrils. For this particular model of the protofibrils, Grasso et al

identified three mechanisms in which ligands can destabilize the protofibrils: inter-chain destabilization, pocket distortion and pocket stabilization [91]. In the present study, we found that the mechanism of destabilization was by the pocket distortion mechanism as defined by Grasso et al [91]. The extent of destabilization was measured by the root mean squared deviation (RMSD), the extent of the β – sheet structure, the hydrogen bonding network and stability of the salt bridges. The RMSD values of the $KLVFFP_5$ – Aβ systems were higher than that of the KLVFF – Aβ systems indicating a greater degree of destabilization. There were fewer residues forming extending β-sheets in the presence of the $KLVFFP_5$ peptide than in the presence of the KLVFF peptide. By forming contacts with the $KLVFFP_5$ peptide the protofibril residues lost their native contacts, leading to the loss of their structure. The $KLVFFP_5$ peptide also had a greater ability to disrupt the hydrogen bonding network and the salt bridges of the protofibrils. The tight interatomic packing of the protofibrils was made looser by the $KLVFFP_5$ peptide. Thus the proline modification of the KLVFF peptide improved its ability to bind to the protofibrils and disrupt their structure.

Conclusions

In the present study the interaction of a designed peptide $KLVFFP_5$ with the amyloid beta protofibrils was investigated. This peptide was designed to exploit the properties of the self-recognition sequence of the amyloid-b peptide KLVFF and the β-sheet breaker amino acid proline. The binding modes of the $KLVFFP_5$ and the destabilization of the amyloid protofibrils were characterized. The mechanism of binding was by the formation of hydrophobic contacts and hydrogen bonds with the protofibril residues. The $KLVFFP_5$ peptide could destabilize the amyloid protofibrils to a greater extent than the KLVFF peptide. In the presence of the $KLVFFP_5$ peptide the protofibrils lost their beta-sheet structure leading to the formation of coils and helices. The hydrogen bonding network of the protofibrils and the salt bridges are critical for protofibril stability. The $KLVFFP_5$ peptide disrupted the hydrogen bonding network and the salt bridges in the protofibrils to a greater extent than the KLVFF peptide. The tight interatomic packing of the protofibrils was made looser by the $KLVFFP_5$ peptide. Our results indicate that the $KLVFFP_5$ peptide is an effective β-sheet disruptor which can be considered in the therapy of Alzheimer's disease.

Declarations

Funding: No funding was received for conducting this study.

Conflicts of Interest: There are no conflicts to declare.

Availability of data and material: N/A

Code availability: N/A

Authors' contributions: Conception and design of study: P.K. Kanchi, A.K. Dasmahapatra. Acquisition of data: P.K. Kanchi. Analysis and interpretation of data: P.K. Kanchi, A.K. Dasmahapatra.

ACKNOWLEDGEMENT

Computational facilities supported by the Department of Science and Technology (SR/S3/CE/0069/2010 and SR/FST/ETII-028/2010), Government of India are highly acknowledged. The authors would also like to acknowledge the high performance computing facility Param Ishan provided by the Indian Institute of Technology Guwahati.

References

1. Querfurth HW, LaFerla FM (2010) Alzheimer's disease. N Engl J Med 362:329–344. https://doi.org/10.1056/NEJMra0909142
2. Ross CA, Poirier MA (2004) Protein aggregation and neurodegenerative disease. Nat Med 10 Suppl:S10-7. https://doi.org/10.1038/nm1066
3. Prusiner SB (2001) Shattuck lecture--neurodegenerative diseases and prions. N Engl J Med 344:1516–1526. https://doi.org/10.1056/NEJM200105173442006
4. Selkoe DJ (2001) Alzheimer's disease: genes, proteins, and therapy. Physiol Rev 81:741–766. https://doi.org/10.1152/physrev.2001.81.2.741
5. Cummings J, Lee G, Ritter A, et al (2019) Alzheimer's disease drug development pipeline: 2019. Alzheimer's Dement (New York, N Y) 5:272–293. https://doi.org/10.1016/j.trci.2019.05.008
6. Man BY-W, Chan H-M, Leung C-H, et al (2011) Group 9 metal-based inhibitors of β-amyloid (1–40) fibrillation as potential therapeutic agents for Alzheimer's disease. Chem Sci 2:917–921. https://doi.org/10.1039/C0SC00636J
7. Raman B, Ban T, Yamaguchi K-I, et al (2005) Metal ion-dependent effects of clioquinol on the fibril growth of an amyloid {beta} peptide. J Biol Chem 280:16157–16162. https://doi.org/10.1074/jbc.M500309200
8. Barnham KJ, Kenche VB, Ciccotosto GD, et al (2008) Platinum-based inhibitors of amyloid-beta as therapeutic agents for Alzheimer's disease. Proc Natl Acad Sci U S A 105:6813–6818. https://doi.org/10.1073/pnas.0800712105
9. Iscen A, Brue CR, Roberts KF, et al (2019) Inhibition of Amyloid-β Aggregation by Cobalt(III) Schiff Base Complexes: A Computational and Experimental Approach. J Am Chem Soc 141:16685–16695. https://doi.org/10.1021/jacs.9b06388
10. Lannfelt L, Blennow K, Zetterberg H, et al (2008) Safety, efficacy, and biomarker findings of PBT2 in targeting Abeta as a modifying therapy for Alzheimer's disease: a phase IIa, double-blind, randomised, placebo-controlled trial. Lancet Neurol 7:779–786. https://doi.org/10.1016/S1474-4422(08)70167-4
11. Doens D, Valdés-Tresanco ME, Vasquez V, et al (2019) Hexahydropyrrolo[2,3-b]indole Compounds as Potential Therapeutics for Alzheimer's Disease. ACS Chem Neurosci 10:4250–4263. https://doi.org/10.1021/acschemneuro.9b00297

12. Shi S, Wang H, Wang J, et al (2020) Semi-synthesis and biological evaluation of flavone hybrids as multifunctional agents for the potential treatment of Alzheimer's disease. Bioorg Chem 100:103917. https://doi.org/10.1016/j.bioorg.2020.103917
13. Ehrnhoefer DE, Bieschke J, Boeddrich A, et al (2008) EGCG redirects amyloidogenic polypeptides into unstructured, off-pathway oligomers. Nat Struct Mol Biol 15:558–566. https://doi.org/10.1038/nsmb.1437
14. Ladiwala ARA, Bhattacharya M, Perchiacca JM, et al (2012) Rational design of potent domain antibody inhibitors of amyloid fibril assembly. Proc Natl Acad Sci U S A 109:19965–19970. https://doi.org/10.1073/pnas.1208797109
15. Salloway S, Sperling R, Fox NC, et al (2014) Two phase 3 trials of bapineuzumab in mild-to-moderate Alzheimer's disease. N Engl J Med 370:322–333. https://doi.org/10.1056/NEJMoa1304839
16. Liu E, Schmidt ME, Margolin R, et al (2015) Amyloid-β 11C-PiB-PET imaging results from 2 randomized bapineuzumab phase 3 AD trials. Neurology 85:692–700. https://doi.org/10.1212/WNL.0000000000001877
17. Doody RS, Thomas RG, Farlow M, et al (2014) Phase 3 trials of solanezumab for mild-to-moderate Alzheimer's disease. N Engl J Med 370:311–321. https://doi.org/10.1056/NEJMoa1312889
18. Panza F, Lozupone M, Logroscino G, Imbimbo BP (2019) A critical appraisal of amyloid-β-targeting therapies for Alzheimer disease. Nat Rev Neurol 15:73–88. https://doi.org/10.1038/s41582-018-0116-6
19. Goyal D, Shuaib S, Mann S, Goyal B (2017) Rationally Designed Peptides and Peptidomimetics as Inhibitors of Amyloid-β (Aβ) Aggregation: Potential Therapeutics of Alzheimer's Disease. ACS Comb Sci 19:55–80. https://doi.org/10.1021/acscombsci.6b00116
20. Craik DJ, Fairlie DP, Liras S, Price D (2013) The future of peptide-based drugs. Chem Biol Drug Des 81:136–147. https://doi.org/10.1111/cbdd.12055
21. Matsunaga Y, Fujii A, Awasthi A, et al (2004) Eight-residue Abeta peptides inhibit the aggregation and enzymatic activity of Abeta42. Regul Pept 120:227–236. https://doi.org/10.1016/j.regpep.2004.03.013
22. Tjernberg LO, Näslund J, Lindqvist F, et al (1996) Arrest of beta-amyloid fibril formation by a pentapeptide ligand. J Biol Chem 271:8545–8548. https://doi.org/10.1074/jbc.271.15.8545
23. Soto C, Sigurdsson EM, Morelli L, et al (1998) Beta-sheet breaker peptides inhibit fibrillogenesis in a rat brain model of amyloidosis: implications for Alzheimer's therapy. Nat Med 4:822–826. https://doi.org/10.1038/nm0798-822
24. Lowe TL, Strzelec A, Kiessling LL, Murphy RM (2001) Structure-function relationships for inhibitors of beta-amyloid toxicity containing the recognition sequence KLVFF. Biochemistry 40:7882–7889. https://doi.org/10.1021/bi002734u
25. Kapurniotu A, Buck A, Weber M, et al (2003) Conformational restriction via cyclization in beta-amyloid peptide Abeta(1-28) leads to an inhibitor of Abeta(1-28) amyloidogenesis and cytotoxicity. Chem Biol 10:149–159. https://doi.org/10.1016/s1074-5521(03)00022-x

26. Austen BM, Paleologou KE, Ali SAE, et al (2008) Designing peptide inhibitors for oligomerization and toxicity of Alzheimer's beta-amyloid peptide. Biochemistry 47:1984–1992. https://doi.org/10.1021/bi701415b
27. Findeis MA, Lee JJ, Kelley M, et al (2001) Characterization of cholyl-leu-val-phe-phe-ala-OH as an inhibitor of amyloid beta-peptide polymerization. Amyloid Int J Exp Clin Investig Off J Int Soc Amyloidosis 8:231–241. https://doi.org/10.3109/13506120108993819
28. Poduslo JF, Curran GL, Kumar A, et al (1999) Beta-sheet breaker peptide inhibitor of Alzheimer's amyloidogenesis with increased blood-brain barrier permeability and resistance to proteolytic degradation in plasma. J Neurobiol 39:371–382
29. Poduslo JF, Curran GL (1996) Polyamine Modification Increases the Permeability of Proteins at the Blood-Nerve and Blood-Brain Barriers. J Neurochem 66:1599–1609. https://doi.org/https://doi.org/10.1046/j.1471-4159.1996.66041599.x
30. Gordon DJ, Sciarretta KL, Meredith SC (2001) Inhibition of beta-amyloid(40) fibrillogenesis and disassembly of beta-amyloid(40) fibrils by short beta-amyloid congeners containing N-methyl amino acids at alternate residues. Biochemistry 40:8237–8245. https://doi.org/10.1021/bi002416v
31. Gordon DJ, Tappe R, Meredith SC (2002) Design and characterization of a membrane permeable N-methyl amino acid-containing peptide that inhibits Abeta1-40 fibrillogenesis. J Pept Res 60:37–55. https://doi.org/10.1034/j.1399-3011.2002.11002.x
32. Cruz M, Tusell JM, Grillo-Bosch D, et al (2004) Inhibition of beta-amyloid toxicity by short peptides containing N-methyl amino acids. J Pept Res 63:324–328. https://doi.org/10.1111/j.1399-3011.2004.00156.x
33. Grillo-Bosch D, Carulla N, Cruz M, et al (2009) Retro-enantio N-methylated peptides as beta-amyloid aggregation inhibitors. ChemMedChem 4:1488–1494. https://doi.org/10.1002/cmdc.200900191
34. Findeis MA (2002) Peptide inhibitors of beta amyloid aggregation. Curr Top Med Chem 2:417–423. https://doi.org/10.2174/1568026024607508
35. Chalifour RJ, McLaughlin RW, Lavoie L, et al (2003) Stereoselective interactions of peptide inhibitors with the beta-amyloid peptide. J Biol Chem 278:34874–34881. https://doi.org/10.1074/jbc.M212694200
36. Jagota S, Rajadas J (2013) Synthesis of d-amino acid peptides and their effect on beta-amyloid aggregation and toxicity in transgenic Caenorhabditis elegans. Med Chem Res 22:3991–4000. https://doi.org/10.1007/s00044-012-0386-2
37. Watanabe K, Nakamura K, Akikusa S, et al (2002) Inhibitors of Fibril Formation and Cytotoxicity of β-Amyloid Peptide Composed of KLVFF Recognition Element and Flexible Hydrophilic Disrupting Element. Biochem Biophys Res Commun 290:121–124. https://doi.org/https://doi.org/10.1006/bbrc.2001.6191
38. Amijee H, Bate C, Williams A, et al (2012) The N-Methylated Peptide SEN304 Powerfully Inhibits Aβ(1–42) Toxicity by Perturbing Oligomer Formation. Biochemistry 51:8338–8352. https://doi.org/10.1021/bi300415v

39. Etienne MA, Aucoin JP, Fu Y, et al (2006) Stoichiometric inhibition of amyloid beta-protein aggregation with peptides containing alternating alpha,alpha-disubstituted amino acids. J Am Chem Soc 128:3522–3523. https://doi.org/10.1021/ja0600678
40. Chafekar SM, Malda H, Merkx M, et al (2007) Branched KLVFF tetramers strongly potentiate inhibition of beta-amyloid aggregation. Chembiochem 8:1857–1864. https://doi.org/10.1002/cbic.200700338
41. Rocha S, Cardoso I, Börner H, et al (2009) Design and biological activity of beta-sheet breaker peptide conjugates. Biochem Biophys Res Commun 380:397–401. https://doi.org/10.1016/j.bbrc.2009.01.090
42. Viet MH, Siposova K, Bednarikova Z, et al (2015) In Silico and in Vitro Study of Binding Affinity of Tripeptides to Amyloid β Fibrils: Implications for Alzheimer's Disease. J Phys Chem B 119:5145–5155. https://doi.org/10.1021/acs.jpcb.5b00006
43. Gladkevich A, Bosker F, Korf J, et al (2007) Proline-rich polypeptides in Alzheimer's disease and neurodegenerative disorders – therapeutic potential or a mirage? Prog Neuropsychopharmacol Biol Psychiatry 31:1347–1355. https://doi.org/10.1016/j.pnpbp.2007.06.005
44. Bilikiewicz A, Gaus W (2004) Colostrinin (a naturally occurring, proline-rich, polypeptide mixture) in the treatment of Alzheimer's disease. J Alzheimers Dis 6:17–26. https://doi.org/10.3233/jad-2004-6103
45. Leszek J, Inglot AD, Janusz M, et al (1999) Colostrinin: a proline-rich polypeptide (PRP) complex isolated from ovine colostrum for treatment of Alzheimer's disease. A double-blind, placebo-controlled study. Arch Immunol Ther Exp (Warsz) 47:377–385
46. Yenkoyan K, Safaryan K, Chavushyan V, et al (2011) Neuroprotective action of proline-rich polypeptide-1 in β-amyloid induced neurodegeneration in rats. Brain Res Bull 86:262–271. https://doi.org/10.1016/j.brainresbull.2011.08.003
47. Chou PY, Fasman GD (1974) Prediction of protein conformation. Biochemistry 13:222–245. https://doi.org/10.1021/bi00699a002
48. Wood SJ, Wetzel R, Martin JD, Hurle MR (1995) Prolines and amyloidogenicity in fragments of the Alzheimer's peptide beta/A4. Biochemistry 34:724–730. https://doi.org/10.1021/bi00003a003
49. Herning T, Yutani K, Inaka K, et al (1992) Role of proline residues in human lysozyme stability: a scanning calorimetric study combined with X-ray structure analysis of proline mutants. Biochemistry 31:7077–7085. https://doi.org/10.1021/bi00146a008
50. Rauscher S, Baud S, Miao M, et al (2006) Proline and glycine control protein self-organization into elastomeric or amyloid fibrils. Structure 14:1667–1676. https://doi.org/10.1016/j.str.2006.09.008
51. Xiao Y, Ma B, McElheny D, et al (2015) Aβ(1-42) fibril structure illuminates self-recognition and replication of amyloid in Alzheimer's disease. Nat Struct Mol Biol 22:499–505. https://doi.org/10.1038/nsmb.2991
52. Xiang N, Lyu Y, Zhu X, Narsimhan G (2018) Investigation of the interaction of amyloid β peptide (11–42) oligomers with a 1-palmitoyl-2-oleoyl-sn-glycero-3-phosphocholine (POPC) membrane using

molecular dynamics simulation. Phys Chem Chem Phys 20:6817–6829. https://doi.org/10.1039/C7CP07148E

53. Jahanbin F, Bozorgmehr MR, Morsali A, Beyramabadi SA (2019) The effect of different alcohols on the Asp23-Lys28 and Asp23-Ala42 salt bridges of the most effective peptide in Alzheimer's disease: Molecular dynamics viewpoints. J Mol Graph Model 86:199–208. https://doi.org/10.1016/j.jmgm.2018.10.022
54. Grasso G, Rebella M, Muscat S, et al (2018) Conformational Dynamics and Stability of U-Shaped and S-Shaped Amyloid β Assemblies. Int. J. Mol. Sci. 19
55. Jakubowski JM, Orr AA, Le DA, Tamamis P (2020) Interactions between Curcumin Derivatives and Amyloid-β Fibrils: Insights from Molecular Dynamics Simulations. J Chem Inf Model 60:289–305. https://doi.org/10.1021/acs.jcim.9b00561
56. Zhang M, Zheng J, Nussinov R, Ma B (2018) Molecular Recognition between Aβ-Specific Single-Domain Antibody and Aβ Misfolded Aggregates. Antibodies 7
57. Thai NQ, Nguyen HL, Linh HQ, Li MS (2017) Protocol for fast screening of multi-target drug candidates: Application to Alzheimer's disease. J Mol Graph Model 77:121–129. https://doi.org/https://doi.org/10.1016/j.jmgm.2017.08.002
58. Gautieri A, Beeg M, Gobbi M, et al (2019) The Anti-Amyloidogenic Action of Doxycycline: A Molecular Dynamics Study on the Interaction with Aβ42. Int. J. Mol. Sci. 20
59. Grasso G, Rebella M, Morbiducci U, et al (2019) The Role of Structural Polymorphism in Driving the Mechanical Performance of the Alzheimer's Beta Amyloid Fibrils. Front Bioeng Biotechnol 7:83. https://doi.org/10.3389/fbioe.2019.00083
60. Villalobos Acosta DMÁ, Chimal Vega B, Correa Basurto J, et al (2018) Recent Advances by In Silico and In Vitro Studies of Amyloid-β 1-42 Fibril Depicted a S-Shape Conformation. Int J Mol Sci 19:2415. https://doi.org/10.3390/ijms19082415
61. Hou S, Gu R-X, Wei D-Q (2017) Inhibition of β-Amyloid Channels with a Drug Candidate wgx-50 Revealed by Molecular Dynamics Simulations. J Chem Inf Model 57:2811–2821. https://doi.org/10.1021/acs.jcim.7b00452
62. Fan H-M, Gu R-X, Wang Y-J, et al (2015) Destabilization of Alzheimer's Aβ42 Protofibrils with a Novel Drug Candidate wgx-50 by Molecular Dynamics Simulations. J Phys Chem B 119:11196–11202. https://doi.org/10.1021/acs.jpcb.5b03116
63. Battisti A, Palumbo Piccionello A, Sgarbossa A, et al (2017) Curcumin-like compounds designed to modify amyloid beta peptide aggregation patterns. RSC Adv 7:31714–31724. https://doi.org/10.1039/C7RA05300B
64. Xi W, Wang W, Abbott G, Hansmann UHE (2016) Stability of a Recently Found Triple-β-Stranded Aβ1-42 Fibril Motif. J Phys Chem B 120:4548–4557. https://doi.org/10.1021/acs.jpcb.6b01724
65. Bitan G, Kirkitadze MD, Lomakin A, et al (2003) Amyloid beta -protein (Abeta) assembly: Abeta 40 and Abeta 42 oligomerize through distinct pathways. Proc Natl Acad Sci U S A 100:330–335. https://doi.org/10.1073/pnas.222681699

66. Cheon M, Kang M, Chang I (2016) Polymorphism of fibrillar structures depending on the size of assembled Aβ17-42 peptides. Sci Rep 6:38196. https://doi.org/10.1038/srep38196
67. Kahler A, Sticht H, Horn AHC (2013) Conformational Stability of Fibrillar Amyloid-Beta Oligomers via Protofilament Pair Formation – A Systematic Computational Study. PLoS One 8:e70521
68. Kozakov D, Brenke R, Comeau SR, Vajda S (2006) PIPER: an FFT-based protein docking program with pairwise potentials. Proteins 65:392–406. https://doi.org/10.1002/prot.21117
69. Kozakov D, Beglov D, Bohnuud T, et al (2013) How good is automated protein docking? Proteins 81:2159–2166. https://doi.org/10.1002/prot.24403
70. Kozakov D, Hall DR, Xia B, et al (2017) The ClusPro web server for protein-protein docking. Nat Protoc 12:255–278. https://doi.org/10.1038/nprot.2016.169
71. Comeau SR, Gatchell DW, Vajda S, Camacho CJ (2004) ClusPro: an automated docking and discrimination method for the prediction of protein complexes. Bioinformatics 20:45–50. https://doi.org/10.1093/bioinformatics/btg371
72. Comeau SR, Gatchell DW, Vajda S, Camacho CJ (2004) ClusPro: a fully automated algorithm for protein-protein docking. Nucleic Acids Res 32:W96-9. https://doi.org/10.1093/nar/gkh354
73. Nosé S (1984) A unified formulation of the constant temperature molecular dynamics methods. J Chem Phys 81:511–519. https://doi.org/10.1063/1.447334
74. Hoover WG (1985) Canonical dynamics: Equilibrium phase-space distributions. Phys Rev A, Gen Phys 31:1695–1697. https://doi.org/10.1103/physreva.31.1695
75. Parrinello M, Rahman A (1981) Polymorphic transitions in single crystals: A new molecular dynamics method. J Appl Phys 52:7182–7190. https://doi.org/10.1063/1.328693
76. Nosé S, Klein ML (1983) Constant pressure molecular dynamics for molecular systems. Mol Phys 50:1055–1076. https://doi.org/10.1080/00268978300102851
77. Abraham MJ, Murtola T, Schulz R, et al (2015) GROMACS: High performance molecular simulations through multi-level parallelism from laptops to supercomputers. SoftwareX 1–2:19–25. https://doi.org/https://doi.org/10.1016/j.softx.2015.06.001
78. Hess B (2008) P-LINCS: A Parallel Linear Constraint Solver for Molecular Simulation. J Chem Theory Comput 4:116–122. https://doi.org/10.1021/ct700200b
79. Essmann U, Perera L, Berkowitz ML, et al (1995) A smooth particle mesh Ewald method. J Chem Phys 103:8577–8593. https://doi.org/10.1063/1.470117
80. Touw WG, Baakman C, Black J, et al (2015) A series of PDB-related databanks for everyday needs. Nucleic Acids Res 43:D364–D368. https://doi.org/10.1093/nar/gku1028
81. Kabsch W, Sander C (1983) Dictionary of protein secondary structure: pattern recognition of hydrogen-bonded and geometrical features. Biopolymers 22:2577–2637. https://doi.org/10.1002/bip.360221211
82. van der Spoel D, van Maaren PJ, Larsson P, Tîmneanu N (2006) Thermodynamics of hydrogen bonding in hydrophilic and hydrophobic media. J Phys Chem B 110:4393–4398.

https://doi.org/10.1021/jp0572535

83. Eisenhaber F, Lijnzaad P, Argos P, et al (1995) The double cubic lattice method: Efficient approaches to numerical integration of surface area and volume and to dot surface contouring of molecular assemblies. J Comput Chem 16:273–284. https://doi.org/https://doi.org/10.1002/jcc.540160303
84. Srinivasan J, Miller J, Kollman PA, Case DA (1998) Continuum solvent studies of the stability of RNA hairpin loops and helices. J Biomol Struct Dyn 16:671–682. https://doi.org/10.1080/07391102.1998.10508279
85. Kollman PA, Massova I, Reyes C, et al (2000) Calculating Structures and Free Energies of Complex Molecules: Combining Molecular Mechanics and Continuum Models. Acc Chem Res 33:889–897. https://doi.org/10.1021/ar000033j
86. Kumari R, Kumar R, Lynn A (2014) g_mmpbsa–a GROMACS tool for high-throughput MM-PBSA calculations. J Chem Inf Model 54:1951–1962. https://doi.org/10.1021/ci500020m
87. Baker NA, Sept D, Joseph S, et al (2001) Electrostatics of nanosystems: application to microtubules and the ribosome. Proc Natl Acad Sci U S A 98:10037–10041. https://doi.org/10.1073/pnas.181342398
88. Tian W, Chen C, Lei X, et al (2018) CASTp 3.0: computed atlas of surface topography of proteins. Nucleic Acids Res 46:W363–W367. https://doi.org/10.1093/nar/gky473
89. Kozlovskii I, Popov P (2020) Spatiotemporal identification of druggable binding sites using deep learning. Commun Biol 3:618. https://doi.org/10.1038/s42003-020-01350-0
90. Singh T, Biswas D, Jayaram B (2011) AADS–an automated active site identification, docking, and scoring protocol for protein targets based on physicochemical descriptors. J Chem Inf Model 51:2515–2527. https://doi.org/10.1021/ci200193z
91. Muscat S, Pallante L, Stojceski F, et al (2020) The Impact of Natural Compounds on S-Shaped Aβ42 Fibril: From Molecular Docking to Biophysical Characterization. Int J Mol Sci 21:2017. https://doi.org/10.3390/ijms21062017
92. Kumar S, Tsai CJ, Ma B, Nussinov R (2000) Contribution of salt bridges toward protein thermostability. J Biomol Struct Dyn 17 Suppl 1:79–85. https://doi.org/10.1080/07391102.2000.10506606

Figures

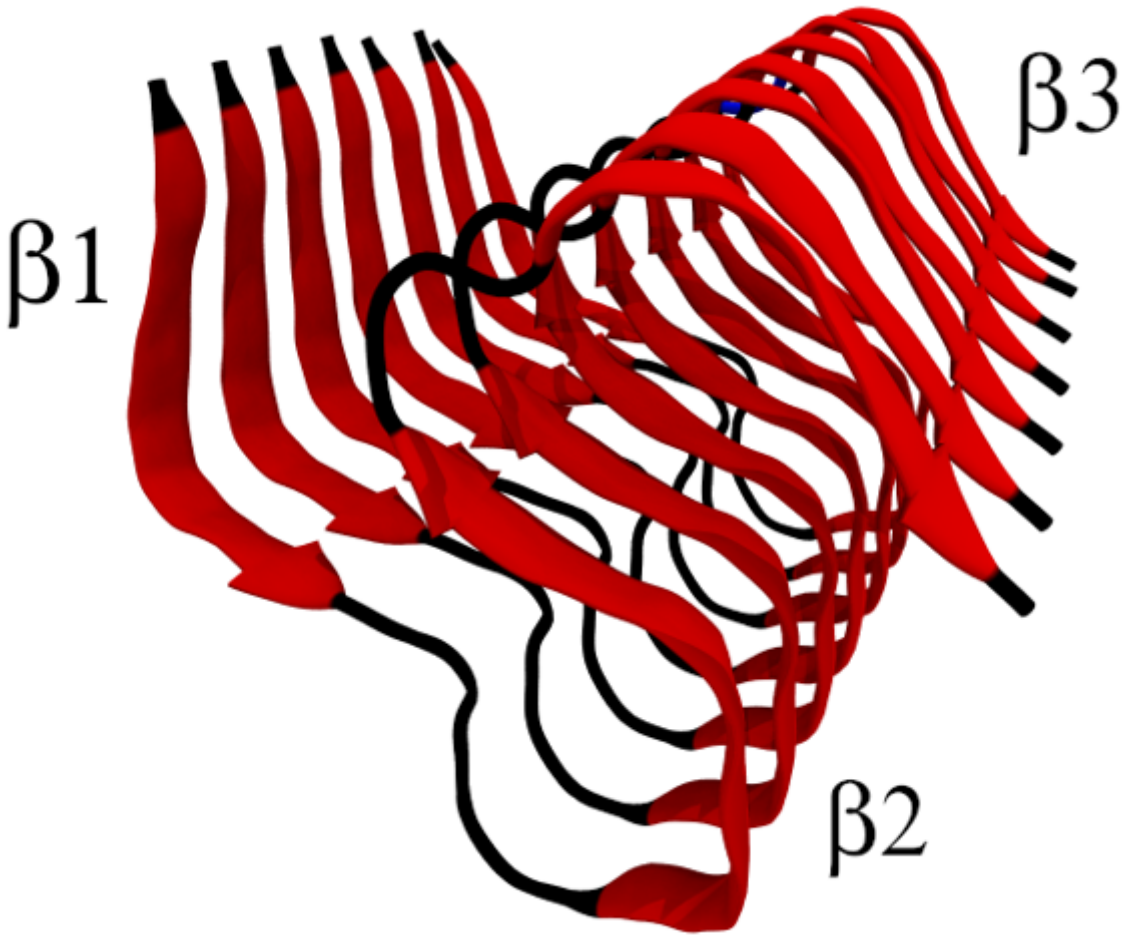

Figure 1

The protofibril model consists of three regions of extended beta-sheet structure shown in red color denoted by β1, β2, and β3. These regions are connected by two loop regions shown in black color.

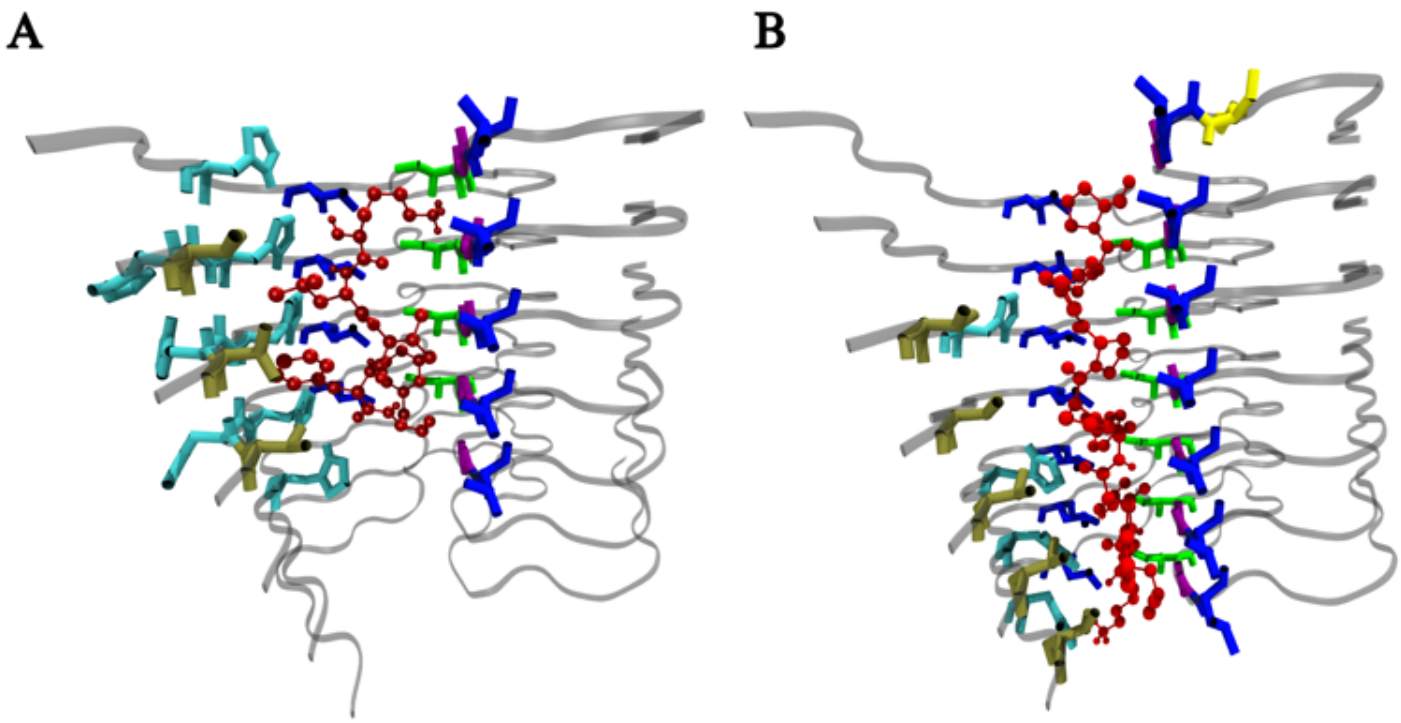

Figure 2

Initial docked structure of the A. K systems and B. KP systems. The Aβ protofibrils are shown as ribbons. The ligands are shown in the CPK representation in red. The protofibril residues which were within 5 of the ligands are shown as bonds. Val 12 is shown in tan color, His 13 and His 14 in cyan, Leu 17 and Leu 34 in blue, Ile 32 in green, Gly 33 in purple and Met 35 in yellow color.

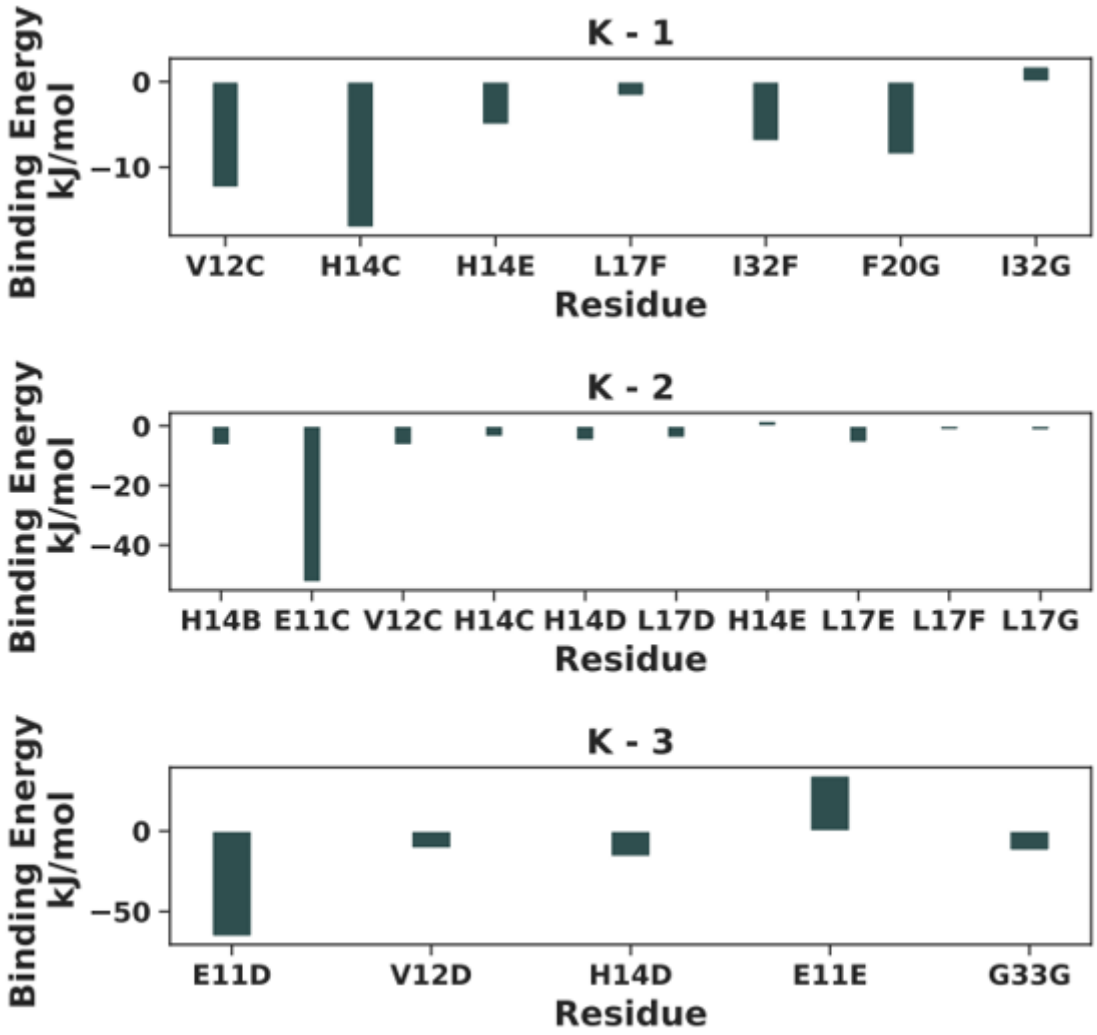

Figure 3

The residues which made sustained contacts with the protofibril residues were the most important for binding. The energetic contribution of these residues to the binding energy in the last 30 ns of the K – 1, K – 2, and K – 3 systems is shown here.

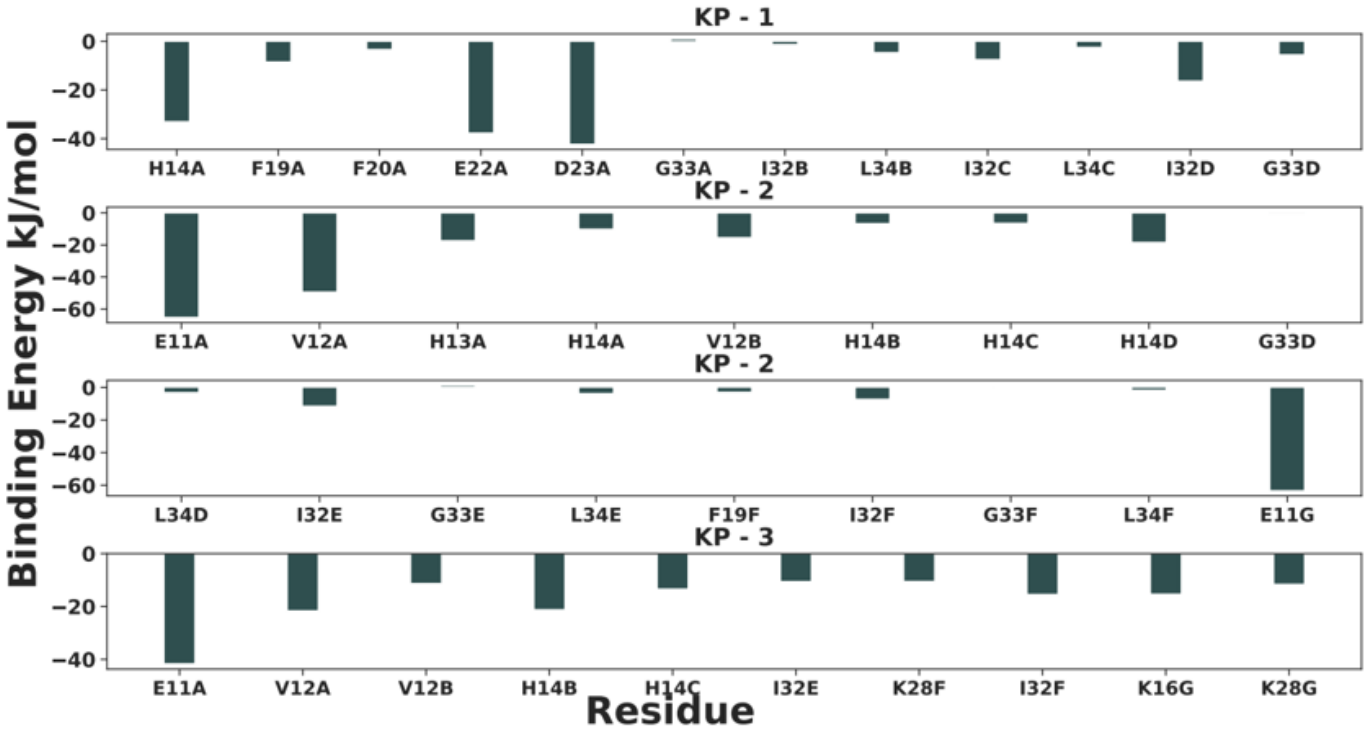

Figure 4

The residues which made sustained contacts with the protofibril residues were the most important for binding. The energetic contribution of these residues to the binding energy in the last 30 ns of the KP – 1, KP – 2, and K – 3 systems is shown here.

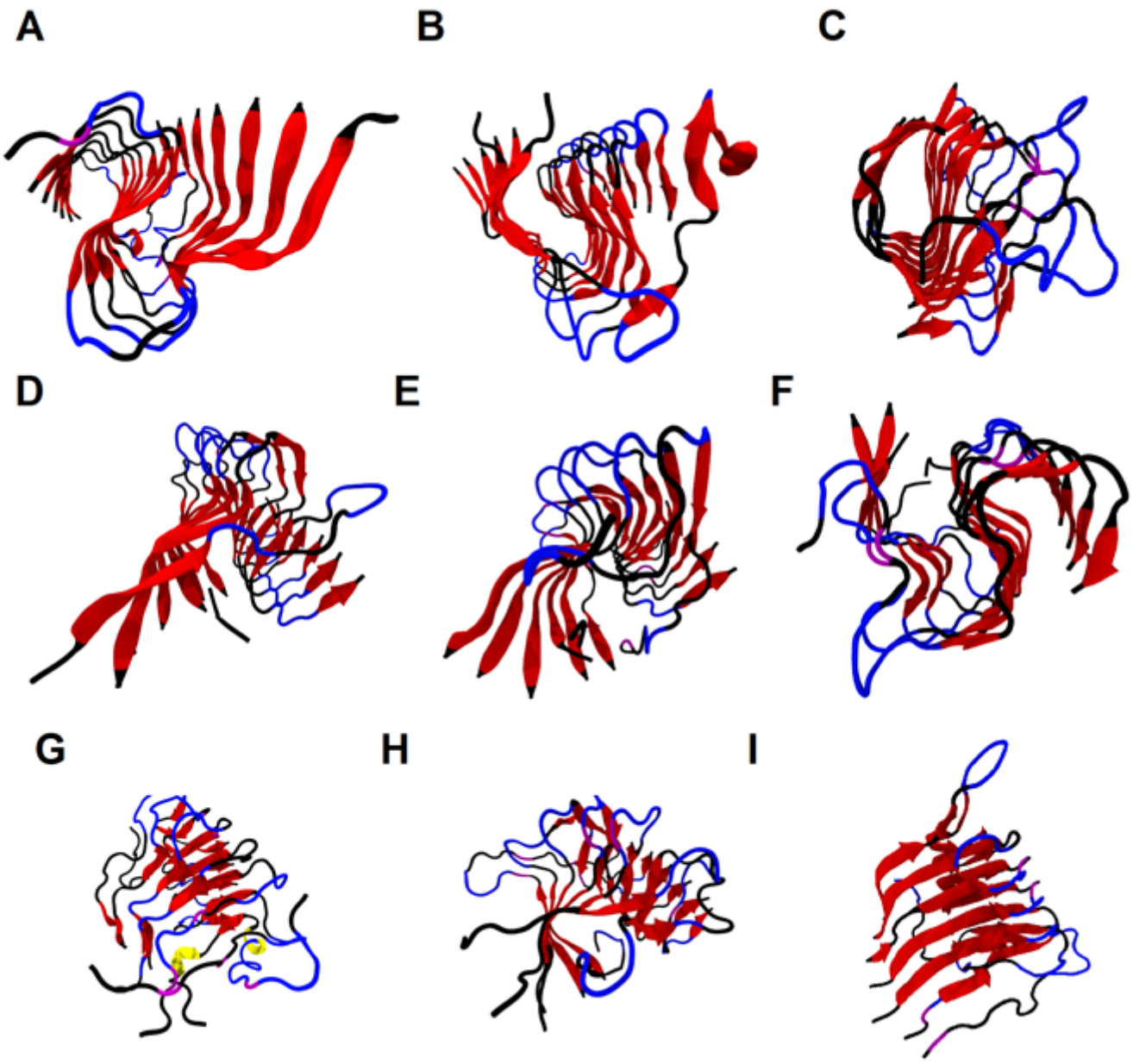

Figure 5

Snapshots of the systems at the end of the simulations, i.e., at the end of 1μs. A. C – 1 system. B. C – 2 system. C. C – 3 system. D. K – 1 system. E. K – 2 system. F. K – 3 system. G. KP – 1 system. H. KP – 2 system. I. KP – 3 system. In the presence of the KLVFFP5 peptide, the extent of destabilization of the protofibrils was the maximum (the KP – 3 system being an outlier). Extended β-sheet regions are shown in red color, turn regions in blue, random coils in black, helices in yellow and bridge-β in purple color.

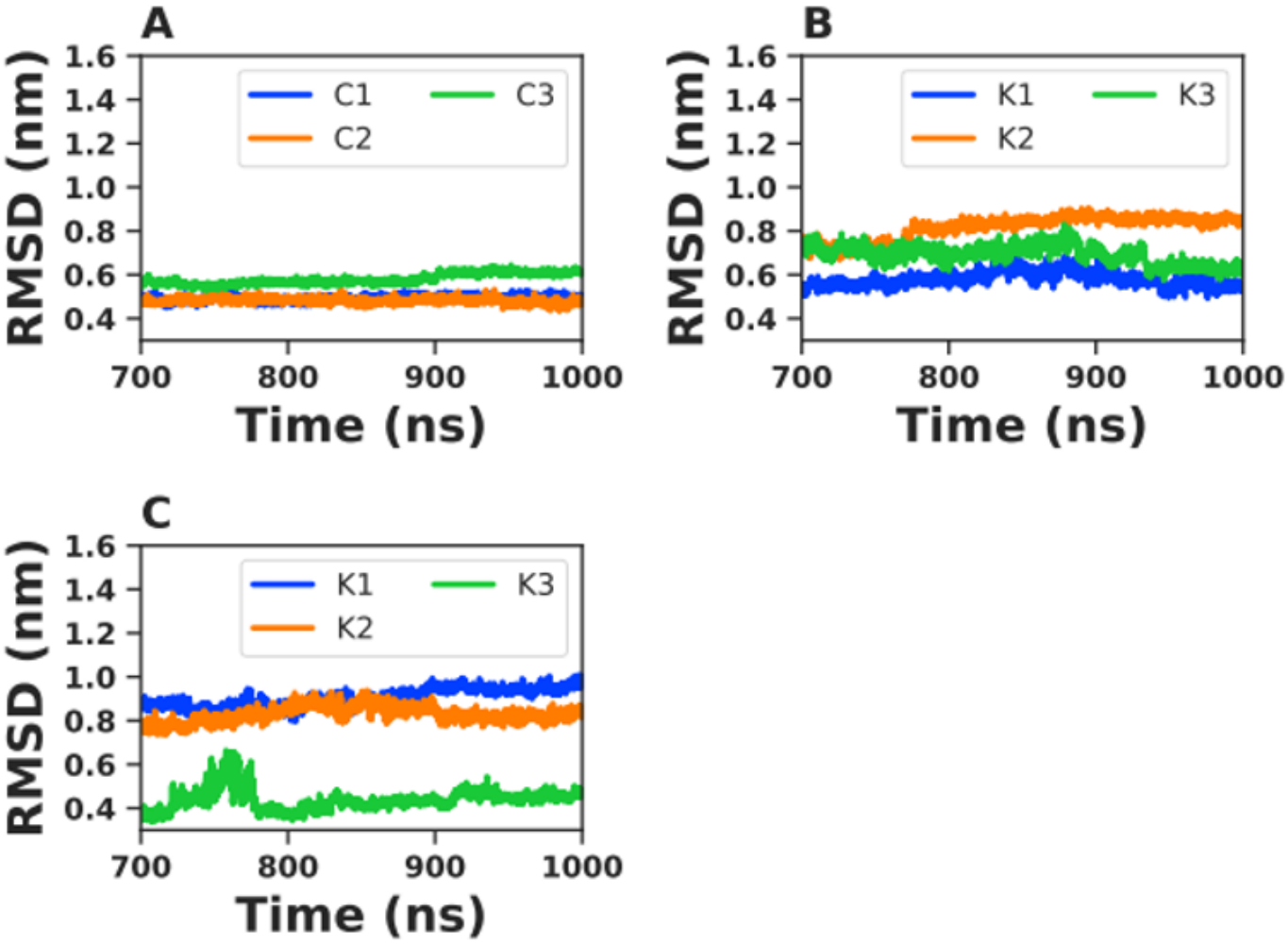

Figure 6

Root-mean squared deviation (RMSD) of the Cα atoms of the Aβ protofibrils in all the systems considered. The values of the KP – 1 and KP – 2 systems were higher than the K systems, indicating a greater extent of destabilization of the protofibrils.

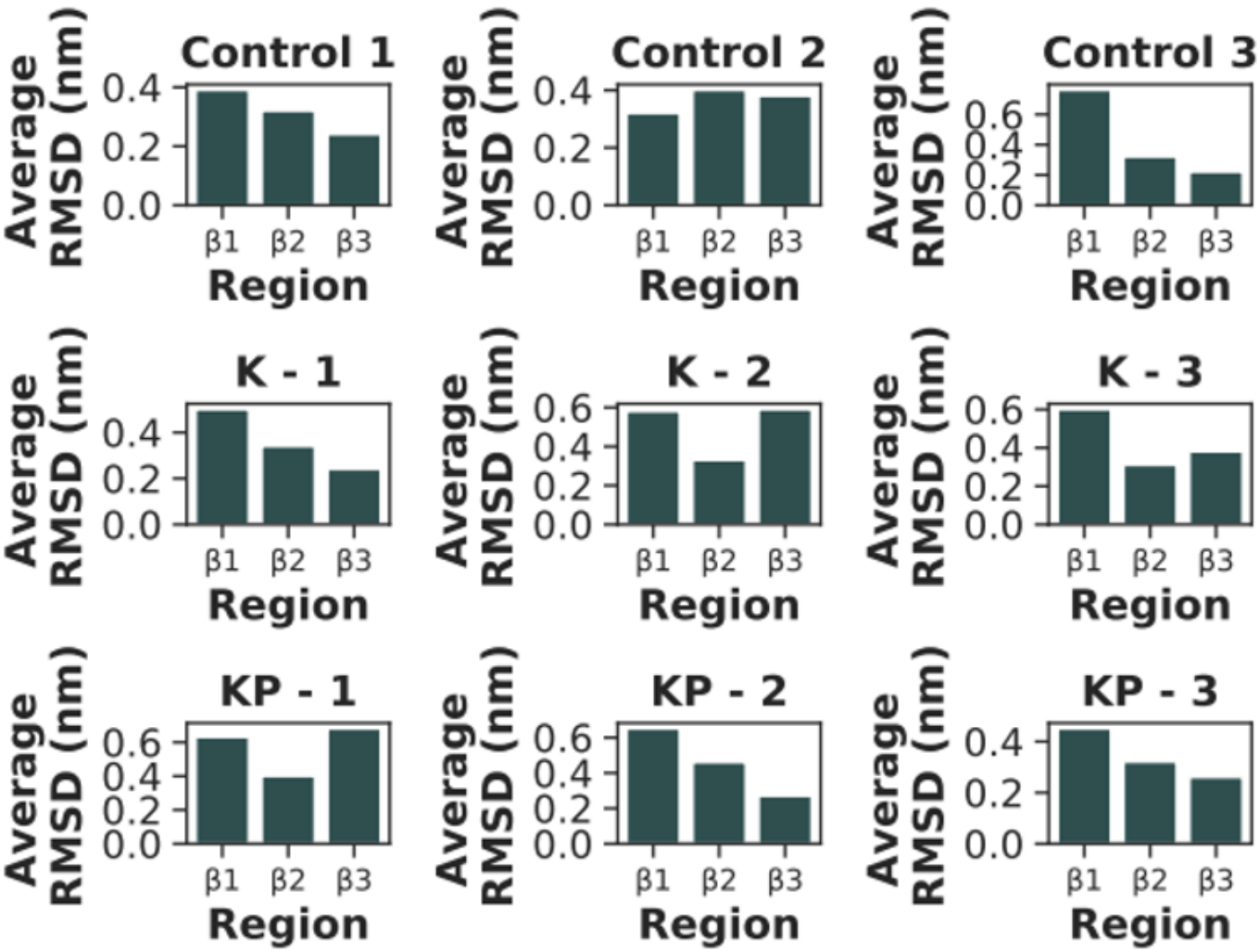

Figure 7

The average RMSD values in the last 300 ns of the different extended β-sheet regions. The β-1 region was destabilized the most by the KLVFFP5 peptide.

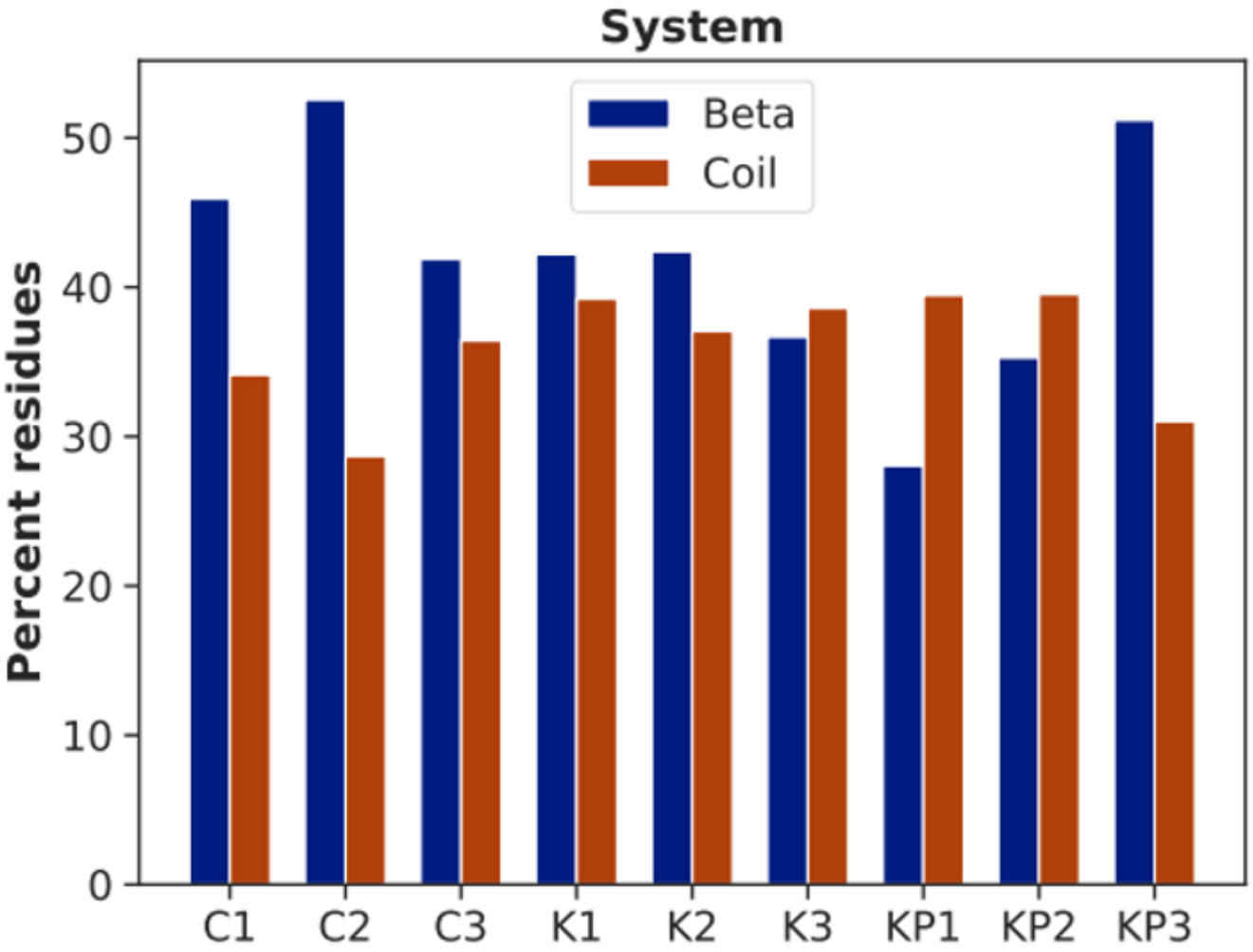

Figure 8

The percent of protofibril residues which formed β-sheets and coils in the systems considered. In the presence of the KLVFF peptide, the β-sheet content of the protofibrils reduced, and in the presence of the KLVFFP5 peptide, it reduced even further indicating the increased destabilization of the protofibrils. With a reduction in the beta-sheet content, there was an associated increase of the number of residues which formed coils.

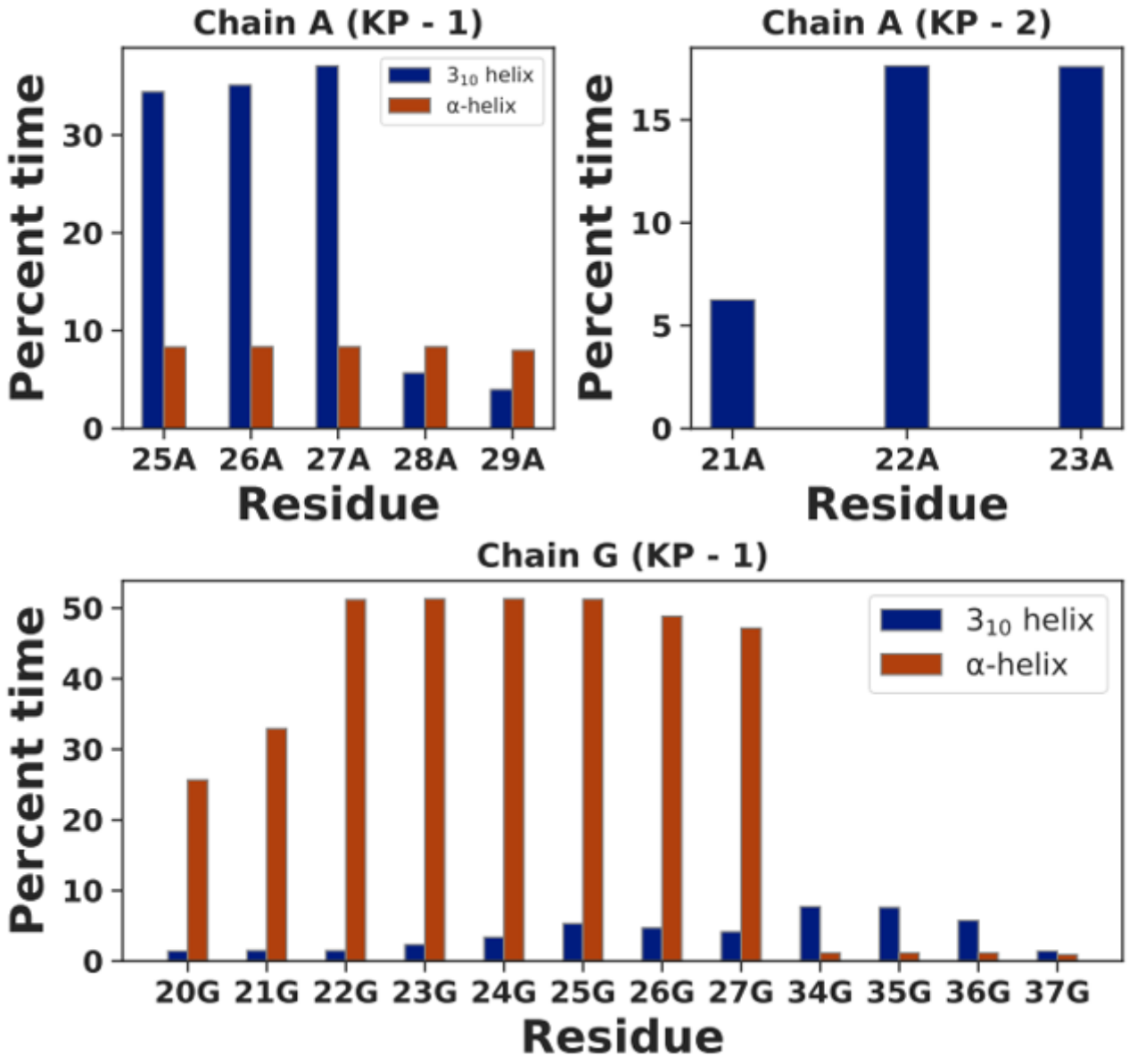

Figure 9

The residues which participated in the formation of helices and their associated durations. In chain A of the KP systems, 310 helices were observed. In chain G of the KP – 1 system, α-helices existed for a significant period of time.

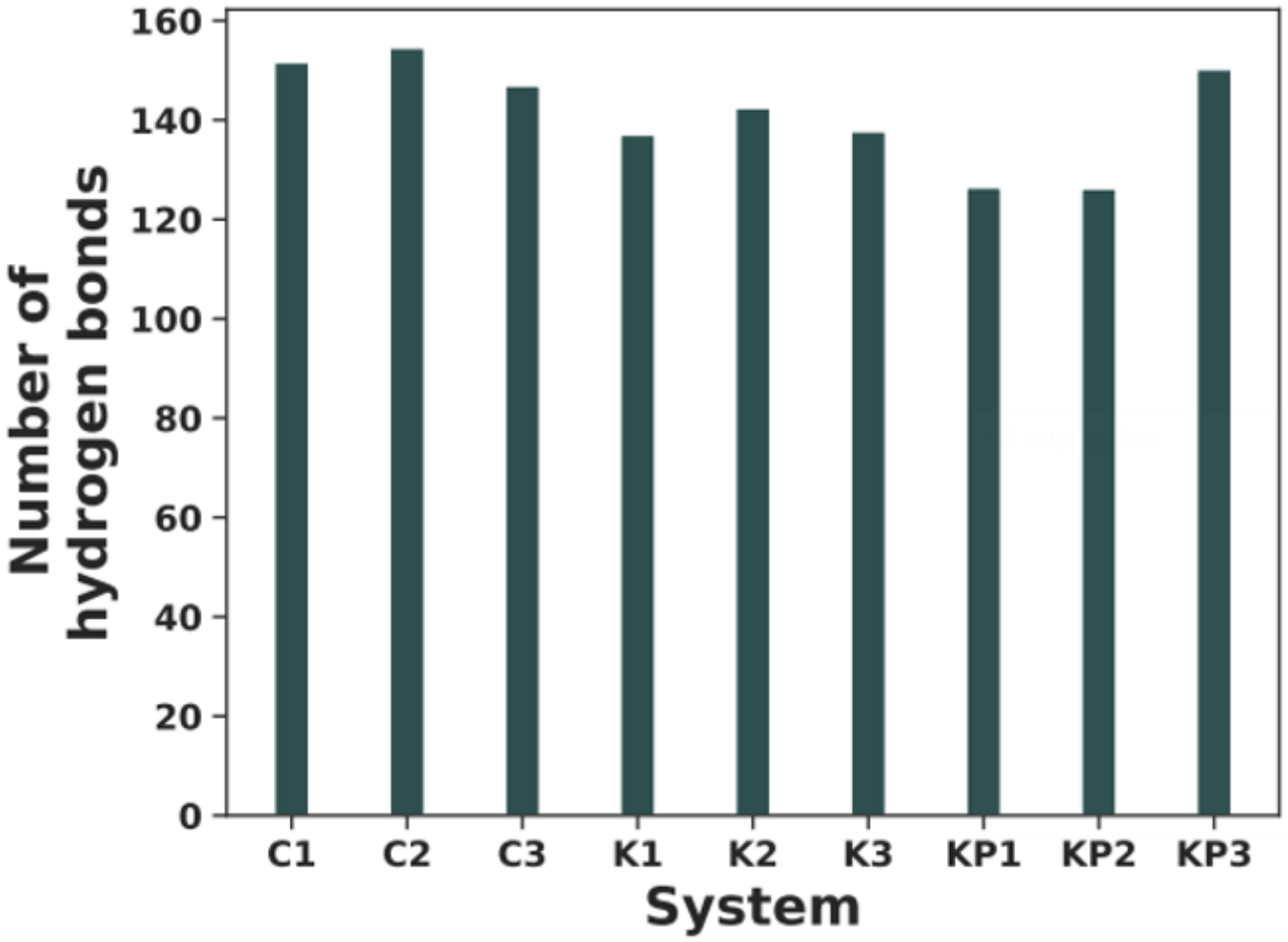

Figure 10

The average number of hydrogen bonds in the protofibrils in all the systems. In the KP – 1 and KP – 2 systems the reduction of hydrogen bonds in the protofibrils was more drastic than in the KLVFF systems.

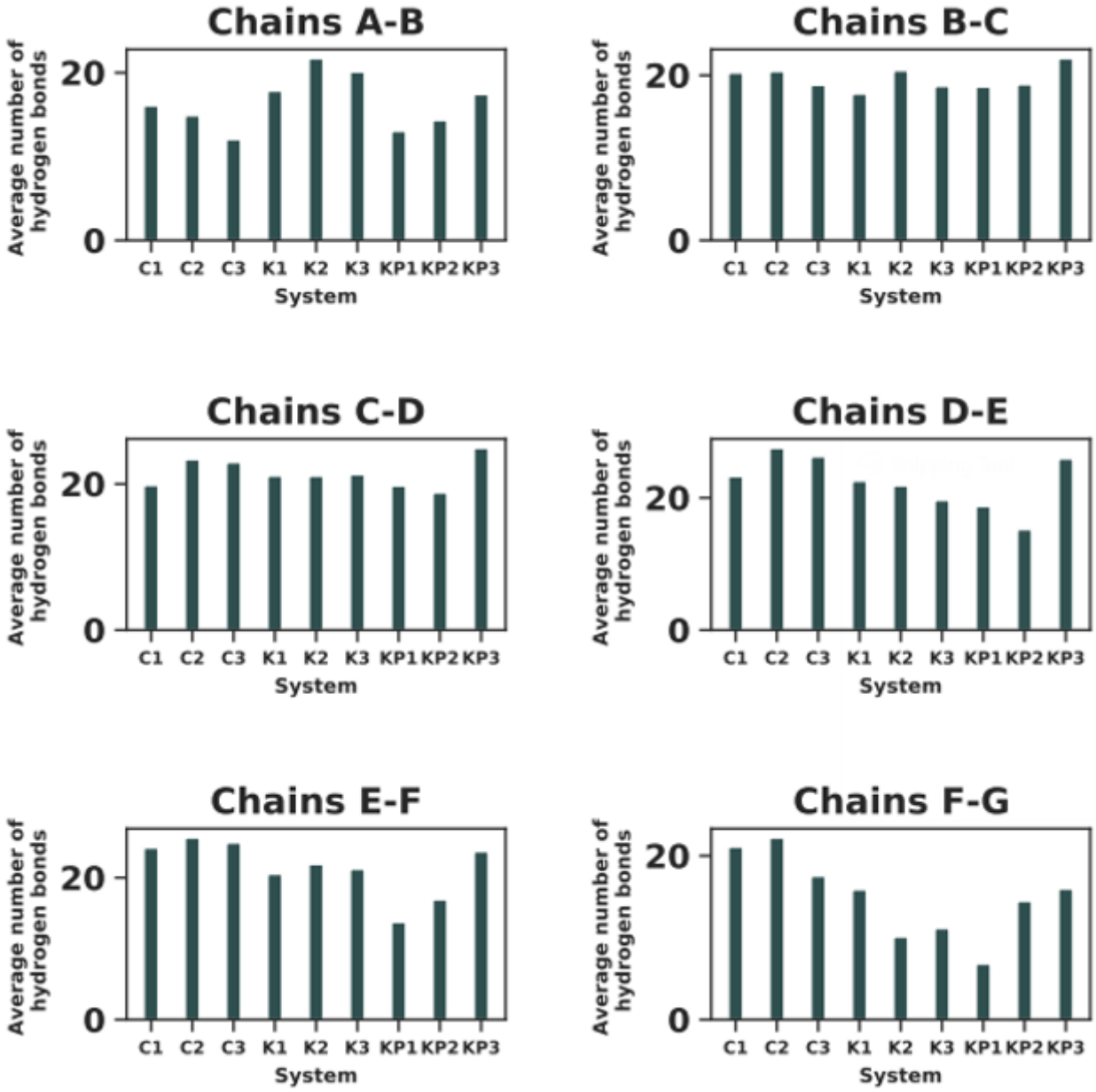

Figure 11

The average number of interchain hydrogen bonds. The interchain hydrogen bonds D-E, E-F, and FG were disrupted in the protofibrils. The KLVFFP5 peptide disrupted the hydrogen bonds between these chains to a greater extent than the KLVFF peptide in the KP – 1 and KP – 2 systems.

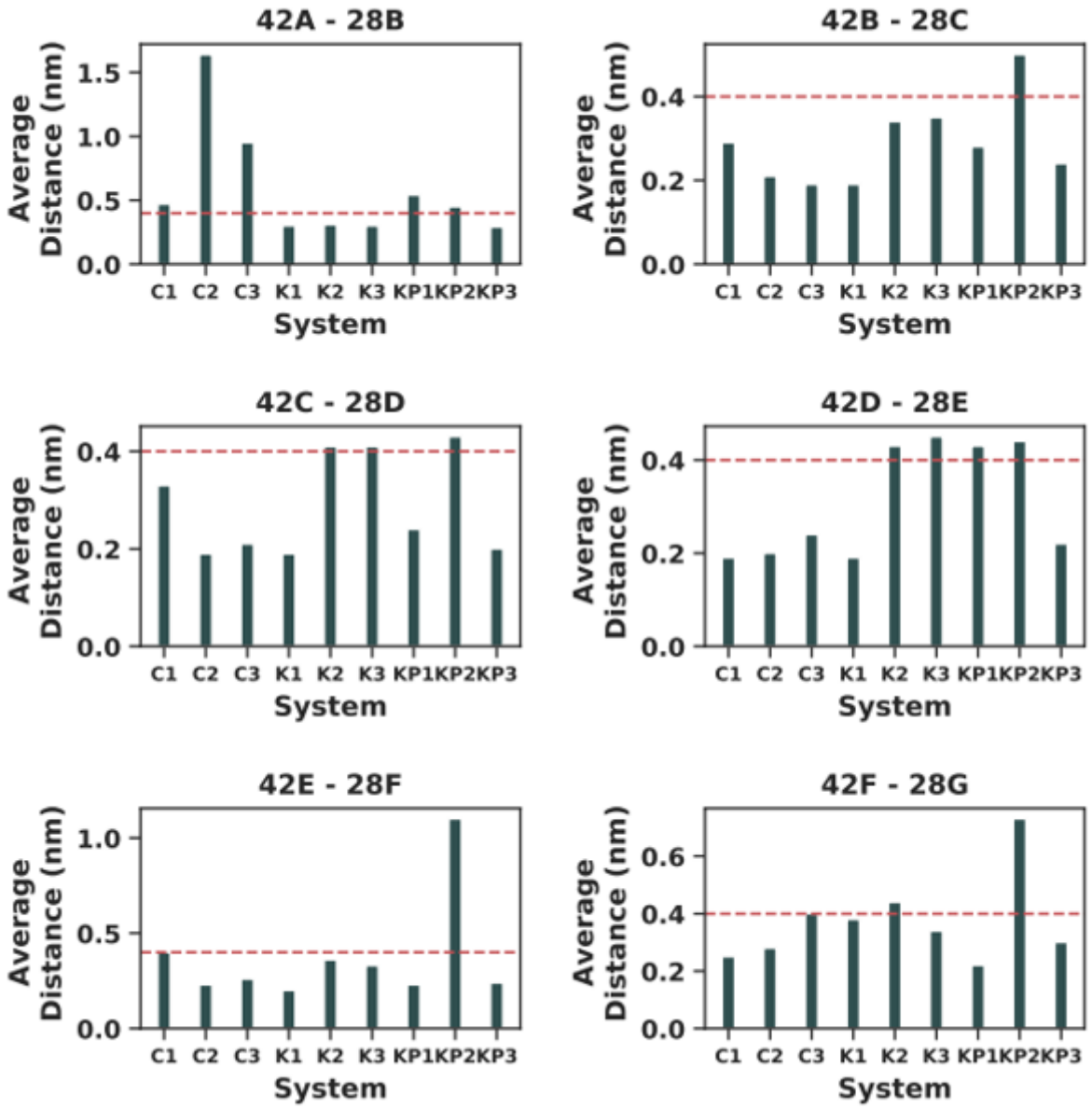

Figure 12

The average distance between the salt bridge forming pairs Ala 42 and Lys 28 in all the systems considered. The red dashed line indicates the cut-off distance for the existence of a salt-bridge. The KLVFFP5 peptide could destabilize all the salt bridges in the KP – 1 and KP – 2 systems.

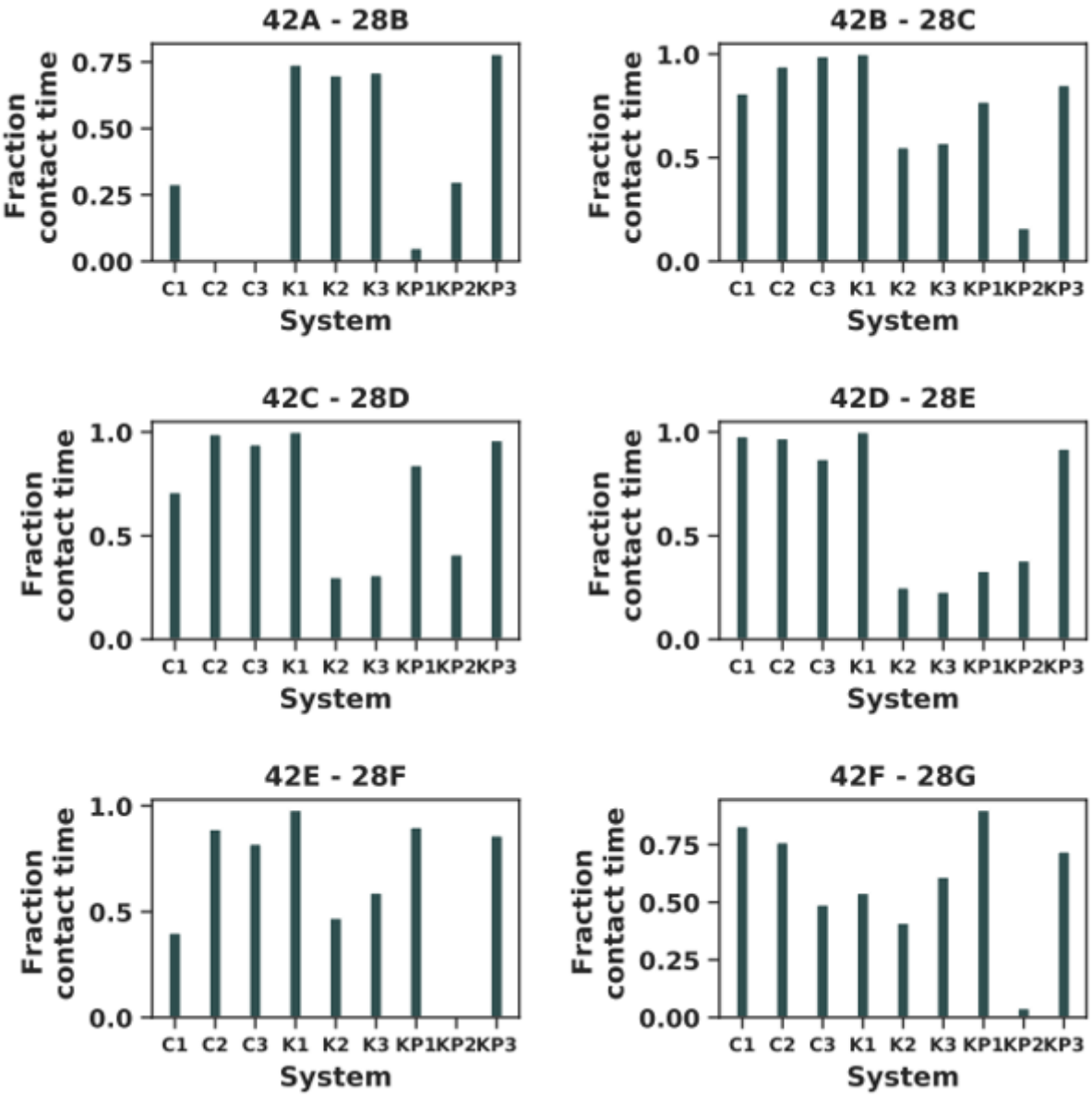

Figure 13

The fraction of time in which the salt-bridge forming residue pairs Ala 42 and Lys 28 were within the cut-off distance of 4Å of each other. In the KP – 1 and KP – 2 systems, these pairs were in contact for a significantly reduced fraction of time, indicating the weakening of the salt-bridges.